4

Simulations

4.1 Beam core and beam halo generations

The beam core and beam halo are generated using Monte Carlo method. Random numbers are generated to fill in defined distributions for the beam core and beam halo.

Input parameters for the ATF2 beam line are defined from the output parameters of the damping ring. The beam core is generated with a Gaussian distribution up to $\pm 3\sigma$ with β_x=6.85 m and β_y=2.94 m. Beam halo is generated outside the beam core ($< -3\sigma$ and $> 3\sigma$) according to the measured beam halo distribution in 2005 (see Section 3.5.2). For simplicity, the beam halo is generated in polar coordinate using Eq. 4.1 assuming the same parametrisation for x and y:

$$\rho_r = K \times r^{-3.5} \quad with \quad r = \sqrt{x^2 + y^2} \tag{4.1}$$

where K is the normalisation factor to match the beam core and beam halo distribution.

The angular distributions of the beam core and beam halo are calculated according to the solution of the equation of motion (Hill's equation) [88, 89]:

$$u(s) = \sqrt{\epsilon}\sqrt{\beta}cos(\phi - \phi_0) \tag{4.2}$$

and its derivative:

$$u^{'}(s) = -\sqrt{\epsilon}\frac{\alpha}{\sqrt{\beta}}cos(\phi - \phi_0) - \frac{\sqrt{\epsilon}}{\sqrt{\beta}}sin(\phi - \phi_0) \tag{4.3}$$

combining the two equations, an invariant of the motion (Courant-Synder invariant) can be obtained:

$$\gamma u^2 + 2\alpha u u' + \beta u'^2 = \epsilon \quad with \quad \gamma = \sqrt{\frac{1+\alpha^2}{\beta}} \tag{4.4}$$

Therefore, the angular distribution of the beam can be generated either according to Eq. 4.3 or Eq. 4.4.

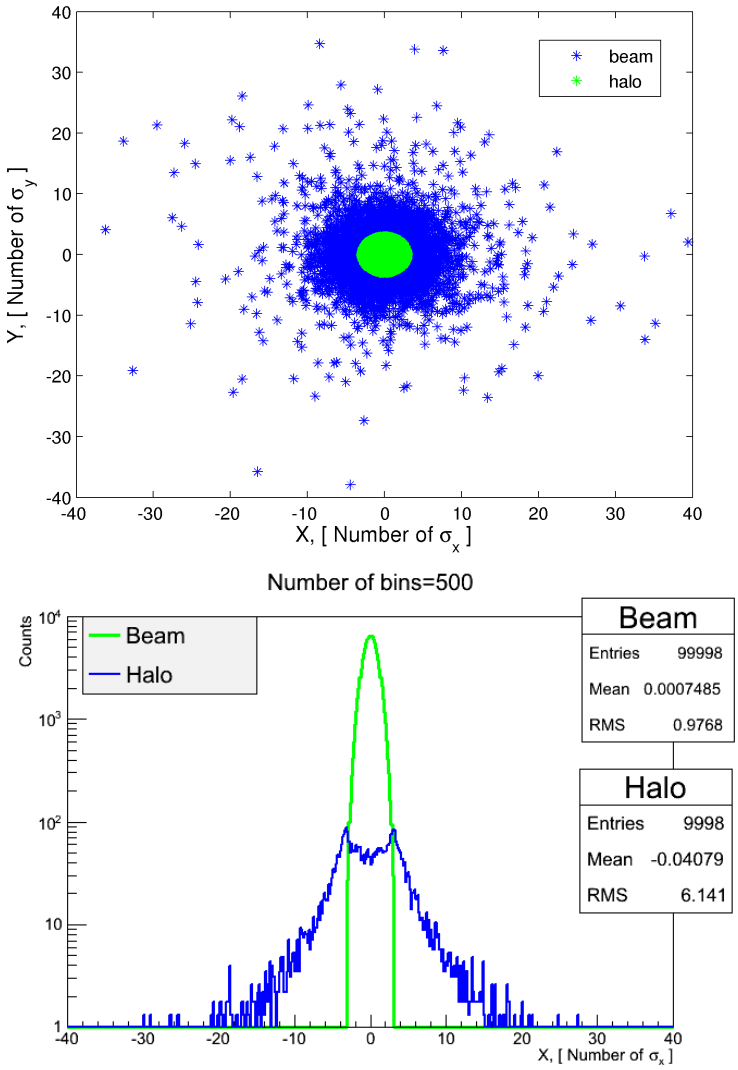

Figure 4.1: Beam core ($N_c = 10^5$) and beam halo ($N_h = 10^4$) distribution profile (upper) and histogram (lower)

An example of the generated beam core and beam halo distribution profile and histogram in number of $\sigma_{x,y}$ is shown in Fig. 4.1. In order to increase the statistics for beam halo, in the simulation, we generated $N_h = 10^4$ of beam halo up to $\pm 40\sigma_{x,y}$, while the beam core is generated up to $\pm 3\sigma_{x,y}$ with the number $N_c = 10^5$ [1].

4.2 Compton recoil electron generations

The Comptons are generated using a software called CAIN [90], which was developed by K.Yokoya at KEK for the study of e^- and e^+ beam-beam interaction and their interaction with a laser. CAIN is a code written in FORTRAN and it uses the Monte-Carlo algorithm to calculate the beam-beam interactions for electrons, positrons and photons including the linear and non-linear Compton scatterings.

Quantum electrodynamic processes (QED) including Compton scattering, Breit-Wheeler process[2] can be added in the program for the laser particle interaction. In our simulation, we are interested only in the Compton scattering process. Linear and nonlinear Compton scattering processes can be chosen for the simulation.

The input parameters used in the simulation are the same ones as listed in Table. 3.4. The electron beam Twiss parameters are defined in the program according to the nominal Twiss parameters at the IP.

In the simulation, macro-particles with a certain particle weight[3] are generated. These macro-particles undergo the Compton scattering process with the calculated probability, and when the Compton scattering happens, one new macro-particle is generated to represent the generated photon.

In the output files, the parameters including generation, weight, space-time location of the particle, energy-momentum, Stokes parameters[4] are provided for each macro-particle.

In our simulation, 10^4 macro-electrons with a weight of 10^6 are used to present the real number of electrons (10^{10}) in the beam. As a result, 360 macro-photons with a

[1] In reality, N_h is estimated to be $0^{-3} of \mathrm{N}_c$.

[2] The Breit-Wheeler process is the emission of positron-electron pairs off a probe photon propagating through a polarized short-pulsed electromagnetic field

[3] The weight of the macro-particles is defined as the ratio between the numbers of real particles and number of macro-particles.

[4] The Stokes parameters are a set of values that describe the polarization state of electromagnetic radiation.

weight of ∼10 are generated for the designed BX1BY1 optics. This number is quite close to the previously calculated expected counts of 3.622×10^3 from Eq. 3.28. Simulations were done also for BX10BY1 optics and BX100BY1000 optics. The estimated counts for different optics are listed in Table 4.1. The estimated counts can serve as a reference for our experiments with different optics. In order to increase the statistics of Comptons, in the tracking simulations, Comptons generated using $E_l = 1.4J$ are used.

BX1BY1 (E_l =1.4 J)	**BX1BY1 (E_l =0.2 J)**	**BX10BY1**	**BX100BY1000**
2.8×10^4	3.6×10^3	3.1×10^3	1.56×10^3

Table 4.1: Expected counts of Compton signal at DS location for different optics

The energy spectrum of Comptons and the input electron beam is shown in Fig. 4.2 for BX1BY1 optics with E_l=1.4 J. It can be seen that most of the Comptons have less energy than the beam and their energy spectrum is much wider than the beam, this permits us to separate them from the beam using the BDUMP bending magnet. The maximum energy loss of the Comptons was calculated in Section 3.6.4 to be 2.27% of the total energy. This result is consistent with the simulated value as shown in Fig. 4.2.

4.3 Tracking of beam halo and Comptons

In order to study the beam halo and Compton spectrum at the DS location, tracking was performed using Mad-X [91] and BDSIM [92].

Mad-X is a program widely used in the field of particle accelerator design and simulation to describe particle accelerators, simulate beam dynamics and optimize beam optics. In this program, parameters like β functions, tune, dispersion, chromaticity can be propagated numerically.

Fig. 4.3 shows the transverse profile of the beam, halo and Compton distributions at the DS location simulated by Mad-X for the BX10BY1 optics. A rectangular shape with sharp edges can be seen on the halo distribution, these edges are caused by the cut of beam halo by the upstream apertures. One of the limits of using Mad-X is that in Mad-X once the electrons hit the aperture of the beam pipe, they are stopped by it, whereas in reality they lose part of their energy by emitting a low momentum bremstrahlung photon and may subsequently remain in the beam pipe. Since such

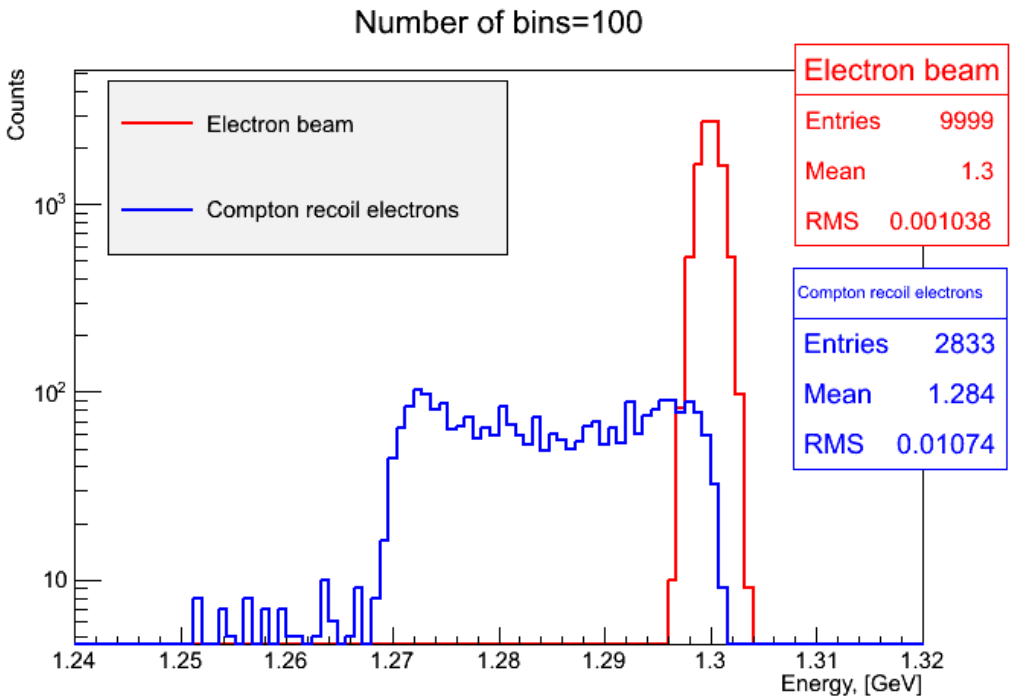

Figure 4.2: Energy spectrum of Compton recoil electrons (blue) and input electron beam (red) for BX1BY1 optics with 1.4 J laser energy

electrons with slightly reduced energies are a source of background for the detection of Comptons, complementary simulations in BDSIM were performed by I. Khvastunov to investigate this background [87].

BDSIM is a GEANT4 [93] based extension toolkit for simulation of particle transport in accelerator beamlines. The simulations were done only for the region from the IP to the DUMP with the BDUMP bending magnet and DS in between and connected to each other using beam pipes.

Fig. 4.4 shows the simulated horizontal halo and Compton distributions at the DS location in Mad-X and in BDSIM. In the Mad-X simulation the total number of halo macro particles was set to 10^4 and then the obtained halo distribution at the DS location was scaled by factor 5.7×10^3 in order to be consistent with the total number of N_h=5.7×10^7 electrons calculated in Ref. [87] for the BDSIM simulation. The Compton distribution is obtained from CAIN with the 1.4 J laser energy setting, therefore total number of Comptons is $\sim2.8\times10^4$ as listed in Table 4.1.

In Mad-X the halo is generated up to $40\sigma_{x,y}$, whereas in BDSIM, different levels of

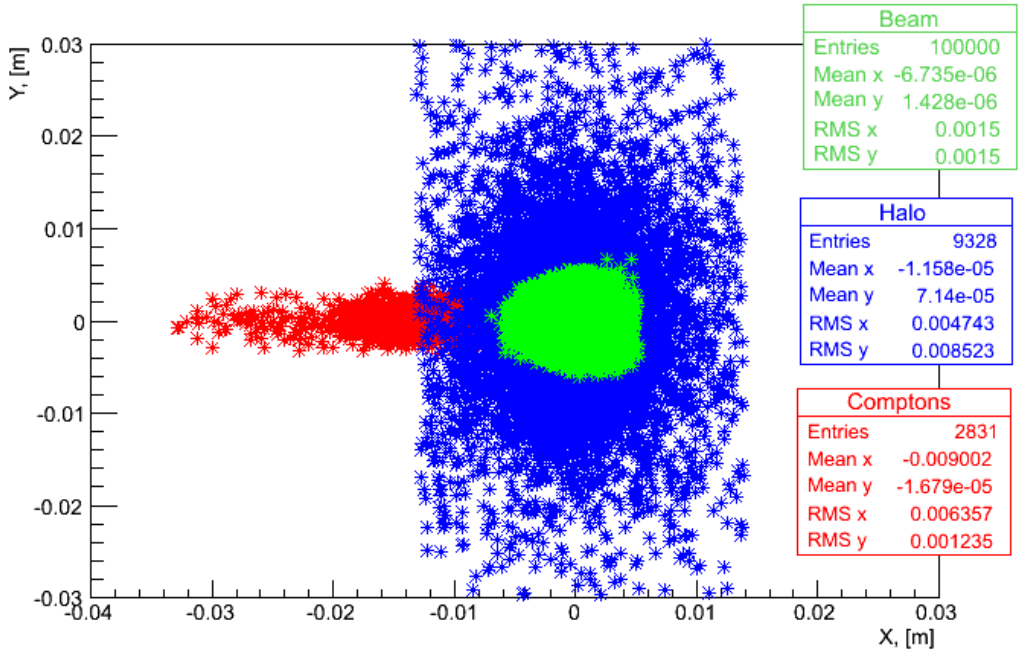

Figure 4.3: Beam (green), halo (blue) and Comptons (red) transverse profile at the DS location for the BX10BY1 optics

halo extension were generated to verify the impact of the electrons with lower energy. From Fig. 4.4 (upper plot) it can seen that in Mad-X the halo is cut by apertures in the beam pipe, therefore even with $40\sigma_{x,y}$ extension it seems the Comptons can be still detected.

In BDSIM, the halos are generated at the IP with angular divergences of $7.5\sigma_{xp}$ and 10-30σ_{yp}. From Fig. 4.4 (lower plot) it can be seen that although with $10\sigma_{yp}$ extension the distribution is similar to the one in Mad-X, an asymmetrical growth of halo can be observed after generating $15\sigma_{yp}$ of halo. More halo is observed on the low energy side than on the high energy side as expected. After adding the beam halo up to 20-30σ_{yp}, the beam halo is dominating the distribution on the low energy side and the Compton signals are covered by the halo in this case. Also an edge at $\pm$50 mm location can be observed which correspond to the cut of beam halo by the aperture of the beam pipe[1]. This information is quite important for the detection of Comptons and can be verified

[1]In the simulation the radius of the beam pipe was set to 50 mm, however, in reality the beam pipe radius is 31.5 mm

in the experiments by measuring the horizontal beam halo distributions. If this is true, then beam halo should be collimated upstream of the IP to certain level (eg. $< 15\sigma_{yp}$) to enable the detection of Comptons.

4.4 Cut of beam halo by apertures

As mentioned in the previous section, the cut of beam halo by the apertures can be verified experimentally, and also can serve as important information for the detection of Comptons. Furthermore, in Mad-X the apertures can be used as "collimators". Therefore, simulations were done to study the cut of beam halo by apertures and to find the best location for collimators.

At present, there is no dedicated beam halo collimator in the ATF2 beamline. However, the apertures of kickers, magnets, BPMs and beam pipes on the beamline can cut the beam halo both in the horizontal and vertical planes. In order to study the beam halo collimation, simulations using MAD-X have been performed to check the cut on the beam halo by the present apertures on the ATF2 beamline.

The beam sizes are shown as a function of positions along the ATF2 beam line in Fig. 4.5. The apertures are shown as a function of positions in unit of sigmas of the beam sizes in the horizontal and vertical directions in Fig. 4.6 (a) and Fig. 4.6 (b), respectively, for the BX10BY1. The vertical apertures for the BX10BY0.5 are also shown in Fig. 4.6 (c).

The BX10BY1 and BX10BY0.5 optics have almost no difference in the scaled horizontal aperture. However in the vertical plane the beam halo is cut less in the BX10BY1 optics than in the BX10BY0.5 optics as the beam size is smaller at the aperture locations. The comparison of cut values is shown in Table 4.2, where several important locations of cut (large beta locations) are indicated.

From the table we can see that the tightest horizontal cut is given by the C-Band BPMs (with radius of 8 mm) installed next to the sextupole SF5FF at 72.23 m from the beginning of the beamline. They introduce a cut on the beam halo at $16.01\sigma_x$. And at DS location, which is 1.35 m from the BDUMPB, the cut is around $25.86\sigma_x$. This cut is caused by the beam pipe installed after the BDUMP with a radius of 31.5 mm. Since the cut of beam halo by the C-Band BPMs is tighter than the cut by the

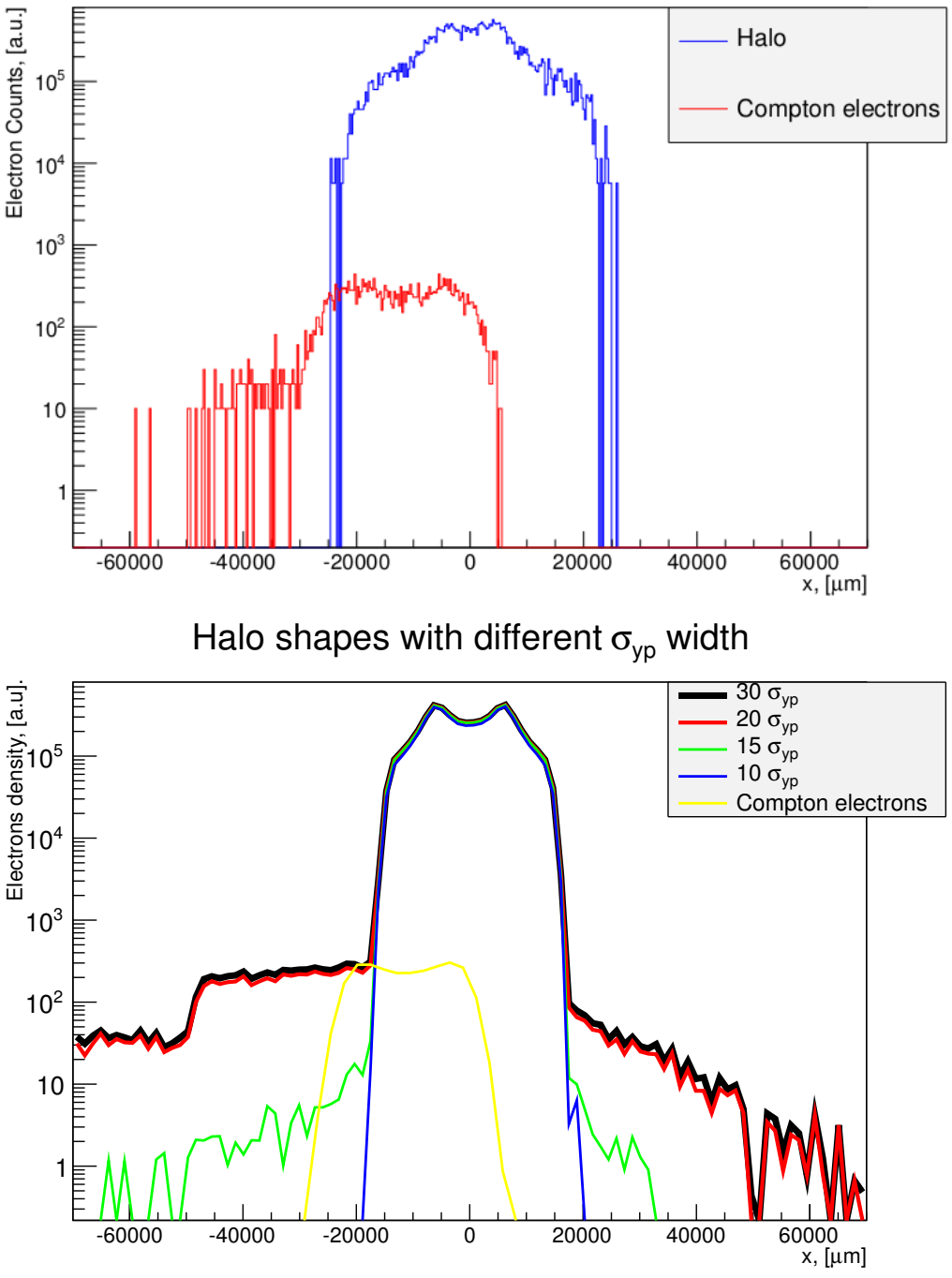

Figure 4.4: Horizontal beam halo and Compton distributions at the DS location simulated using Mad-X (upper) and BDSIM (lower)

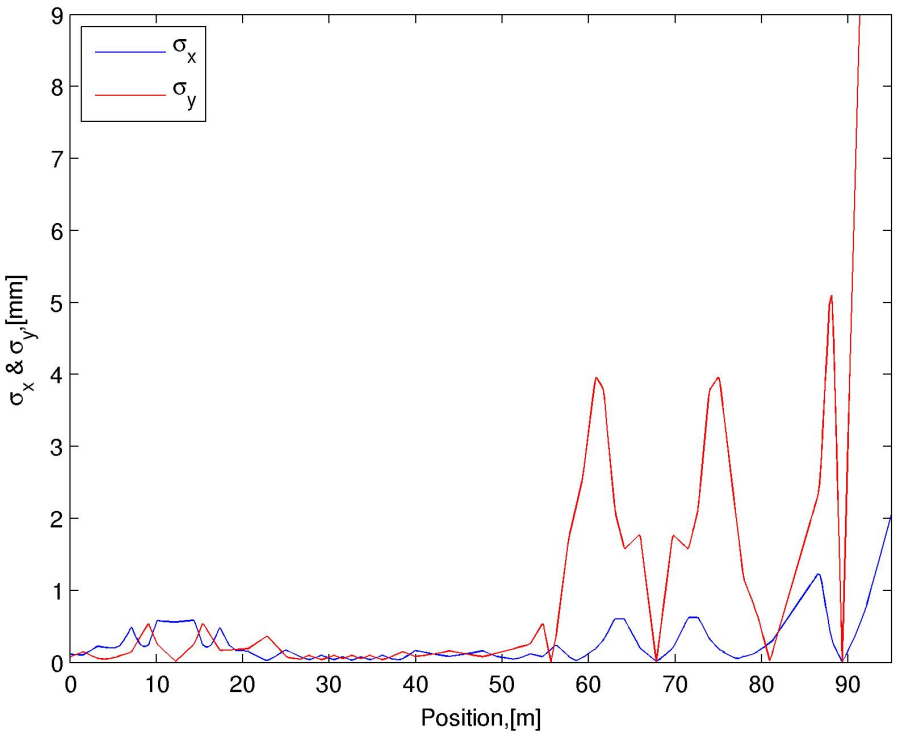

Figure 4.5: Horizontal and vertical beam size along the ATF2 beamline for BX10BY1 optics

beam pipe after BDUMP, we would expect to see this cut on the horizontal beam halo distribution at the DS location.

In the vertical plane, a tappered beam pipe (TBP) was installed at 61.39 m location between the QD10BFF and QD10AFF magnets, where the vertical beam size is very large. The radius of this TBP is 8 mm. It can serve as a collimator for the vertical beam halo to control the background for the beam size measurement using wire scanners or Shintake monitor. The vertical cut by the TBP is estimated to be at $\sim 20\sigma_y$ for BX10BY0.5 optics and $\sim 27\sigma_y$ for BX10BY1 optics.

As the beam is focused to nm scale at the IP, the beam diverges very large after the IP. Thus the tightest vertical cut is given by the BDUMP bending magnet, and at the BDUMPB location, which is the exit of the BDUMP magnet, the cut goes down to $\sim 10\sigma_y$ and $\sim 13\sigma_y$ for the BX10BY0.5 and BX10BY1 optics, respectively. This cut on beam halo may generate large background for beam halo measurement at the

	Horizontal Cut, $[\sigma_x]$		Vertical Cut, $[\sigma_y]$		
	MSF5FF (72.23 m)	DS (93.51 m)	TBP (61.39 m)	BDUMP (92.16 m)	DS (93.51 m)
BX10BY0.5	16.01	25.86	20.06	10.15	20.17
BX10BY1	15.99	25.84	26.85	13.59	26.99

Table 4.2: Cut of beam halo by apertures at large beta locations and expected cut at DS location (in number of $\sigma_{x,y}$)

DS location as shown in the BDSIM simulation in Fig. 4.4. The TBP may be moved vertically to limit this background in the horizontal direction. However, more dedicated beam halo collimation system located upstream are more suited for this purpose [17].

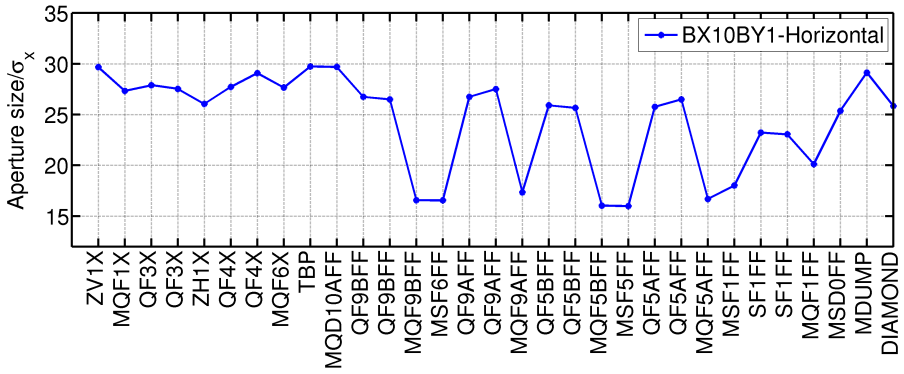

(a)

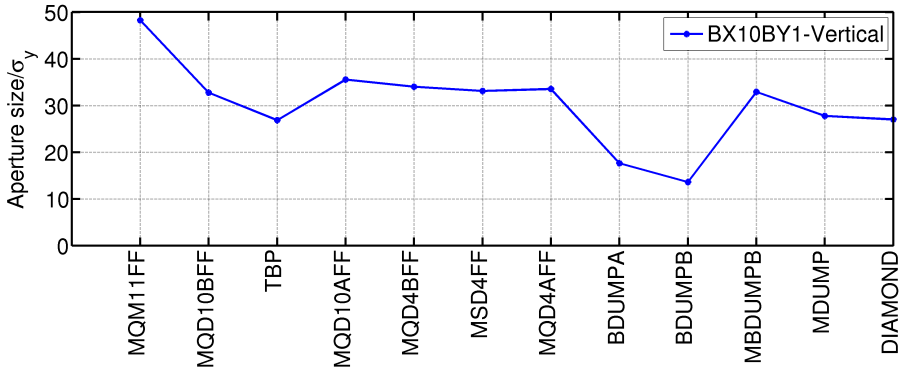

(b)

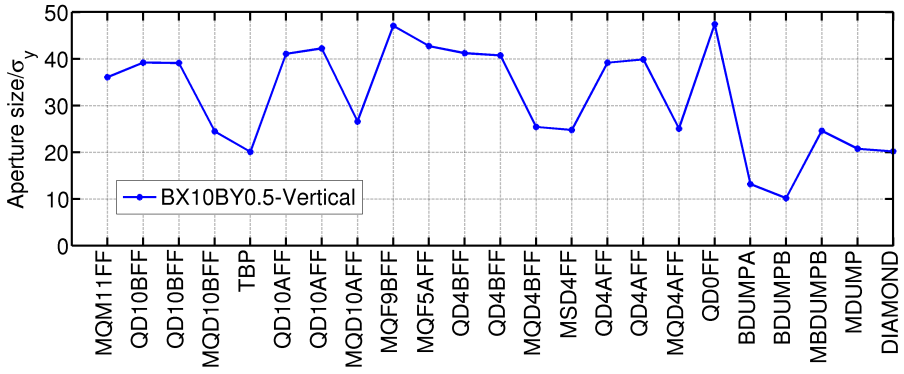

(c)

Figure 4.6: Normalised horizontal apertures as a function of positions for BX10BY1 optics (a); Normalised vertical apertures for BX10BY1 optics (b) and for BX10BY0.5 optics (c). Only positions with a normalised horizontal aperture of less than 30 or with a normalised vertical aperture of less than 50 are shown here.